



Structural models of lipid surface monolayers from X-ray and neutron reflectivity measurements

Manfred Schalke and Mathias Lösche,[‡]

Leipzig University, Institute of Experimental Physics I, Linnéstr. 5, D–04103 Leipzig, Germany

keywords:

lipid membrane models, DMPA, ion binding, lipid headgroup structure, lipid headgroup hydration

ABSTRACT

Structural investigations of phospholipid monolayers on aqueous subphases on the submolecular level using X-ray and neutron reflectivity measurements are reviewed. While such investigations have been limited in the past by a relatively restricted accessible momentum transfer range, recent developments in synchrotron technology – almost doubling this range – have considerably improved the capabilities of the technique. Until recently, data interpretation has entirely relied on „box models“ which describe the structures as molecularly homogeneous slabs – one hydrophobic and one hydrophilic. It is shown that box models of phospholipid monolayers are rather inadequate to model data at the high momentum transfer available nowadays in X-ray measurements. As an alternative, a hybrid data inversion strategy is proposed that treats the hydrophobic alkane phase as a homogeneous slab and describes the position of submolecular fragments of the lipid headgroups by means of distribution functions along the interface. Within this approach, composition-space refinement – enabling the coupling of data sets from various X-ray and neutron contrasts – in connection with volumetric constraints enables structural characterization of lipid monolayers in unprecedented detail.

[‡]To whom correspondence should be addressed.

Extending a recent characterization of DMPA monolayers on pure water [Schalke et al., *Biochim. Biophys. Acta* **1464** (2000), 113] it is shown that stoichiometric binding of the divalent cations – $\text{DMPA}^- : \text{Cat}^{2+} = 2 : 1$ – occurs only at exceedingly low areas per molecule, A_{lipid} . At low surface pressure π , both cations *and* anions are incorporated into the headgroup in significant amounts, $\sim 0.68 \text{ Ba}^{2+}$ and $\sim 0.35 \text{ Cl}^-$ per PA molecule at $\pi = 2 \text{ mN/m}$. They are continuously squeezed out upon compression, until upon approaching $A_{lipid} = 41 \text{ \AA}^2$, the stoichiometric ratio between bound cations and acidic headgroups is observed. The average inclination angle α of the headgroups as well as their water content is constant along the whole isotherm. The intrinsic contribution to the distribution width – *i.e.*, the spread that is due to a distribution of the fragments within the headgroup without the action of capillary waves – increases with compression up to $\pi \sim 30 \text{ mN/m}$ and drops sharply thereafter in a regime of the isotherm where A_{lipid} approaches its limiting value. The same general picture is observed for DMPA on subphases with 10 mM Ca^{2+} , although the lower electron density of that cation limits the precision of the results.

INTRODUCTION

Langmuir monolayers of amphiphilic compounds – such as fatty acids and esters or phospholipids – floating at the air/water interface are frequently investigated objects of research both in materials and life science as well as the physics of low-dimensional systems [1-3]. The most powerful methods to date for the investigation of their structures on a submolecular level are surface sensitive scattering techniques [4-6]: The diffraction of synchrotron X-ray radiation upon grazing incidence (GIXD) and specular reflectivity measurements using X-rays or cold neutron beams. GIXD has obtained extensive attention recently for its unique capabilities in determining the spatial organization of linear alkane compounds in partially ordered – hexatic or crystalline – surface phases [7-10]. It has been considerably boosted by the advent of third generation synchrotron radiation sources [11], which enable high-quality measurements within short illumination times and have also permitted diffraction measurements from more demanding systems such as molecular protein crystal sheets [12-15].

Specular reflectivity measurements in turn reveal information on the electron density distribution along the surface normal. Moreover, utilizing the knowledge of the chemical structure of the film-forming compounds, one may extract information on the three-dimensional organization in a quite general approach, composition-space refinement [16,17]. In distinction from diffraction,

reflectivity measurements are not limited to highly ordered systems but do provide information on molecular subfragments which do not participate in the ordering within a hexatic or crystalline phase – such as the lipid headgroups. Thus, reflection measurements have great potential for probing the static structure of particularly the headgroups in lipid surface monolayers on the submolecular level. This is particularly valuable for investigations of lipid surfaces in a biophysical context: Biomembranes are disordered systems and many physiologically important interactions take place at the interface between the membrane and the aqueous compartment – i.e. at the lipid headgroups.

With the development of synchrotron performance, the quality of X-ray reflectivity measurements has also been dramatically improved by extending the accessible momentum transfer (Q_z) range for systems on aqueous subphases from $Q_z^{\max} \sim 0.5 \text{ \AA}^{-1}$ to $\sim 0.8 \text{ \AA}^{-1}$. This resulted in a considerable gain in resolution of the underlying structures – and required a reexamination of the models used in the past for the evaluation of reflectivity data.

While the so-called two-box model, that has been extensively used to describe the submolecular organization of (phospho-) lipid surface monolayers [1,17-19], has been very well capable of describing X-ray data sets that extend up to $Q_z^{\max} \sim 0.5 \text{ \AA}^{-1}$, such models fail at the description of the high-resolution data available to date [13]. As a consequence, we have developed a novel approach to data modeling [20] that uses distribution functions to describe the organization of submolecular fragments, particularly of phospholipid headgroup substructures, normal to the interface. Such a development has been greatly facilitated by the recent availability of both model-free data inversion techniques [21-23] – enabling an analysis of the inherent weaknesses of the two-box approaches – and volumetric information on lipid substructures from molecular modeling [24,25] – used to reduce the uncertainties in the complex distribution-function model. This contribution reviews the available models of lipid surface monolayers utilized to invert both X-ray and/or neutron reflectivity data and reports new structural details on the binding of divalent cations to the anionic phospholipid dimyristoylphosphatidic acid (DMPA)* in monolayers on aqueous subphases as revealed from high-resolution X-ray reflectivity measurements using the distribution function approach.

*Abbreviations of phospholipid species: DMPA, dimyristylphosphatidic acid; DPPE, dipalmitoylphosphatidylethanolamine; DLPE, dilauroyl-PE; DOPC: dioleoylphosphatidylcholine, PG: phosphatidylglycerol; and of monolayer phases (using the nomenclature introduced by Cadenhead et al. [26]): G, gaseous; LE, liquid expanded; LC, liquid condensed; SC, solid condensed

EXPERIMENTAL PROCEDURES

DMPA, Na⁺ salt, from Sigma (München, Germany) was used as supplied. Water was filtered using a Millipore (Bedford, MA) Milli-Q system, yielding a residual specific resistance of better than 18.2 MΩcm. BaCl₂ and CaCl₂ salts used (Sigma) were of *p.a.* grade. The X-ray reflectivity R of DMPA surface monolayers was determined both at a home-based instrument [27] based on a sealed-tube Cu-K_α source, that provides data up to $Q_z^{\max} \sim 0.65 \text{ \AA}^{-1}/R \sim 3 \times 10^{-9}$ at a wavelength $\lambda \sim 1.54 \text{ \AA}$, and at the undulator beamline BW1 [11] of the DORIS III bypass at HASYLAB, Hamburg (Germany), providing data up to $Q_z^{\max} \sim 0.9 \text{ \AA}^{-1}/R \sim 5 \times 10^{-10}$ at $\lambda \sim 1.3 \text{ \AA}$. We found that beam damage of the surface monolayer is an important issue in the full synchrotron beam (reflectivities at low Q_z have been determined with an attenuated beam), particularly for phospholipid monolayers in the fluid phase. The monolayer was thus continuously shifted underneath the beam footprint to ensure that data were always collected from undamaged areas within the surface film. Reproducibility of the measured data was routinely checked along various fragments of the reflectivity curve.

DATA INVERSION AND MODELING

X-ray and neutron optics at interfaces

The optics of X-rays and neutron beams at surfaces have been extensively dealt with in the literature [5,28,29]. Briefly, the real part of the refraction index n is slightly different from unity – and usually *lower* – for the relevant frequencies, and the imaginary part of n , *i.e.*, the absorption coefficient β , is negligibly small,

$$n = 1 - \delta + i\beta \quad (\text{with } \beta \approx 0) \quad (1).$$

This implies *external* total reflection of a plane wave impinging on a planar, ideally sharp interface between two media with a refractive index of 1 and n , respectively, as long as the incident angle α is below the critical angle

$$\alpha_c = \sqrt{2\delta} = \frac{\sqrt{4\pi\rho_{av}}}{k} = \begin{cases} \frac{\sqrt{2\pi\rho_{el}r_0}}{k} & \text{for X-rays} \\ \frac{\sqrt{4\pi\rho_n}}{k} & \text{for neutrons} \end{cases} \quad (2).$$

Here, $k = 2\pi/\lambda$ is the magnitude of the wavevector, ρ_{av} is the average scattering length density

(SLD) of a molecular-size volume V at the interface, ρ_{el} is electron density, $r_0 = \frac{e^2}{m_e c^2} \approx 2.82 \text{ fm}$ is

the classical Thomson electron radius and $\rho_n = \frac{1}{V} \sum_i v_i b_i$ is the neutron SLD, as computed from the atomic content of V (v atoms of the species i that is characterized by the neutron scattering length b are contained in V). While for X-rays, α_c is always real, it can be imaginary in neutron experiments, *e.g.*, if the beam is reflected from the surface of H₂O (for which $\rho_n < 0$). In this case, there is no Q_z regime of total external reflection. Since δ is of the order of 10^{-5} , α_c is typically in the millidegree range. If one is interested in *specular* reflectivity, the momentum transfer, $\vec{Q} = \vec{k}_{out} - \vec{k}_{in}$, is strictly normal to the interface,

$$Q_z = 2k \sin \alpha = \frac{4\pi}{\lambda} \sin \alpha \quad (3),$$

where in a local coordinate system x and y define the interface and z points to the perpendicular direction. Hence,

$$Q_c = \sqrt{4\pi\rho_{av}} \quad (4)$$

is a quantity characteristic of the medium, since it is independent of the wavelength λ (for example, $Q_c^{X\text{-rays}} \approx 0.0217 \text{ \AA}^{-1}$ for water). From Fresnel's law, neglecting differences between different polarization directions and higher orders in δ which is both justified as $\delta \approx 10^{-5}$, one finds a reflection amplitude $r_{1,2}$ between media with the indices n_1 and n_2

$$r_{1,2} \approx \frac{\alpha - \sqrt{\alpha^2 + 2(\delta_1 - \delta_2)}}{\alpha + \sqrt{\alpha^2 + 2(\delta_1 - \delta_2)}} \approx \frac{Q_{c,1}^2 - Q_{c,2}^2}{4Q_z^2} = \frac{4\pi}{Q_z^2} (\rho_{av,1} - \rho_{av,2}) \quad (5)$$

and a reflectivity

$$R = |r|^2 \quad (6).$$

The Fresnel reflectivity R_F of an ideal surface in vacuum (or air) derives from Eqns. (5) and (6) as

$$R_F \approx \left(\frac{Q_c}{2Q_z} \right)^4 \quad (6a),$$

as long as Q_z is sufficiently large (*e.g.*, $> 5 Q_c$).

In reality, interfaces between two media are not mathematically sharp but graded on the Ångstrom length scale, due to atomic roughness in the case of planar solid state surfaces or thermally excited capillary waves in the case of fluid surfaces. This is usually taken into account by convolution of the step function $\Theta(z - z_0)$, that describes the ideal interface, with a Gaussian, yielding the error function as the relevant profile describing the interface [4]:

$$\Theta(z - z_0) \rightarrow \frac{1}{2} \operatorname{erf}\left(\frac{z - z_0}{\sqrt{2}\sigma}\right) + \frac{1}{2} \quad (7),$$

where $\operatorname{erf}(z) = \frac{2}{\sqrt{\pi}} \int_0^z e^{-t^2} dt$ and σ is a parameter related to the amplitude of the roughness. In comparison with the reflectivity from an ideal interface, the surface roughness (s.r.) leads to a Debye-Waller-like damping of the reflection amplitude,

$$r(\text{w/ s.r.}) = r(\text{w/o s.r.}) \cdot e^{-\frac{Q_z^2 \sigma^2}{2}} \quad (8).$$

If a molecularly thin homogeneous film (index n_2) is located on a semi-infinite substrate (index n_3), reflection according to Eq. (5) occurs at both the front and back faces, giving rise to interference with an intensity pattern in the far field characteristic of the index and the thickness d_2 of the film. The interference originates from a phase factor that takes into account the propagation of the wave in the medium

$$r_{1,2} = \frac{r_2 + r_3 \cdot \exp(2ik_{z,n_2} d_2)}{1 + r_2 r_3 \cdot \exp(2ik_{z,n_2} d_2)} \quad (5a),$$

and the absolute square yields the reflectivity,

$$R = \frac{r_2^2 + r_3^2 + 2r_2 r_3 \cdot \cos(2k_{z,n_2} d_2)}{1 + r_2^2 r_3^2 + 2r_2 r_3 \cdot \cos(2k_{z,n_2} d_2)} \quad (5b).$$

Stratified surface films can obviously be accounted for by recursive application of Eqns. (5), taking into account a global surface roughness by means of Eq. (8), as first suggested by Parratt [30]. Arbitrary SLD profiles at the interface may either be treated by slicing the profiles into a sequence of thin layers and determining the reflectivity by the Parratt recursion algorithm or by the kinematic approximation [4,5,28],

$$\frac{R(Q_z)}{R_F(Q_z)} \approx \frac{1}{\rho_{\text{substrate}}^2} \left| \int \frac{d\rho(z)}{dz} e^{iQ_z z} dz \right|^2 \quad (9),$$

which is only valid for $Q_z > 5 Q_c$ but has the advantages of allowing for any analytical form of $\rho(z)$ while being at the same time more intuitive than the recursion formalism.

As in any scattering experiment, the experimental data cannot be directly translated into the underlying structure because of the „phase problem“, *i.e.*, the loss of phase information upon obtaining the scattered intensities from the amplitudes by using either of Eqns. (6) or (9). Limitations to the data inversion procedures that have been extensively used in the past, as well as recent developments, are in the focus of this review.

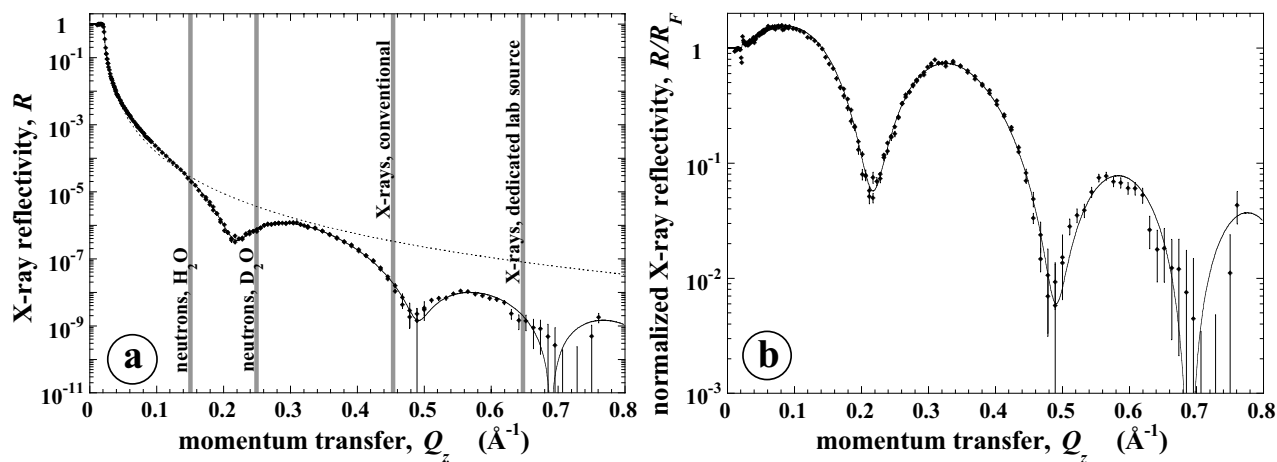


Figure 1: X-ray reflectivity of a DPPE monolayer on water containing 10 mM CaCl_2 at room temperature, $\pi = 28$ mN/m. Continuous lines, derived from a model-free data inversion technique [21], are intended just as guides for the eye. (a) Absolute values of the measured reflectivity. The dotted line indicates the Fresnel reflectivity. Vertical bars indicate the momentum transfer range accessible in typical experimental situations as indicated. Note that the structure of neutron reflectivity data is different from that of X-ray data, particularly with respect to the positions of the minima/maxima due to the different δ -values of the substrate, c.f. Eqns. (1)/(2). (b) Presentation of the same data as in panel (a) in a Fresnel-normalized form which emphasizes the interference effects of the monolayer film and facilitate a critical comparison of experimental data and their model descriptions.

Data quality and resolution

Let us start with analyzing the quality of the available data. As an example, fig. 1 shows the X-ray reflectivity R of a dipalmitoylphosphatidylethanolamin (DPPE) monolayer on an aqueous subphase containing 10 mM CaCl_2 at a lateral pressure $\pi = 28$ mN/m [13], both on an absolute scale together with the Fresnel reflectivity R_F , dotted line, (a) and normalized by R_F (b) which shows more clearly the interference patterns and affords a better comparison of reflectivity data and models. Data have been obtained at BW1/DESY up to $Q_z^{\text{max}} \sim 0.8 \text{ \AA}^{-1}$, where $R \sim 10^{-9}$. Clearly, the signature of the interference is observed in distinct minima of R at $Q_z \sim 0.21 \text{ \AA}^{-1}$, 0.49 \AA^{-1} , and 0.72 \AA^{-1} . Solid lines – computed using a model-free data inversion algorithm (see below) – are intended as guides for the eye. To address the issue of resolution, vertical bars indicate the available maximum momentum transfer of various experimental configurations in comparison to the synchrotron X-ray experiment, which is for neutron reflectometry $Q_z^{\text{max}} \sim 0.15 \text{ \AA}^{-1}$ or 0.25 \AA^{-1} (for H_2O or D_2O subphases, respectively) and $\sim 0.45 \text{ \AA}^{-1} \dots 0.65 \text{ \AA}^{-1}$ for laboratory X-ray sources. This latter range also marks the performance that was routinely obtained until recently in synchrotron experiments (prior to the advent of undulator beamlines), see, *e.g.*, refs. [18,19,31].

A first (and rather conservative) estimate of the limits of resolution in reflectivity measurements is given by the sampling theorem

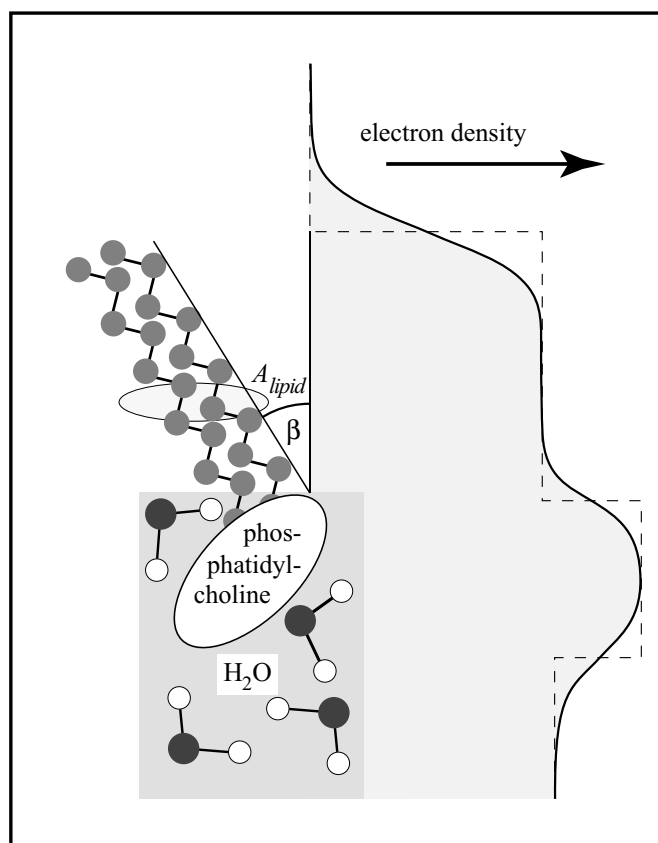
$$\Delta d \sim \frac{\pi}{Q_z^{\max}} \quad (10),$$

which would imply that an intrinsic resolution of $\Delta d \sim 20 \text{ \AA}$ or $\sim 10 \text{ \AA}$ for neutrons on different substrates and between $\Delta d \sim 6 \text{ \AA}$ and $\sim 3 \text{ \AA}$ in X-ray measurements using different radiation sources can be obtained. We will, however, see that molecular fragments may be localized in space with a higher precision if modeling of the data is aided by chemical constraints, the simultaneous use of various (neutron) contrasts, and/or volumetric information on structural subfragments.

Box models

„Box models“ [1,4,5,28] – or layer models – provide a relatively simple, rather intuitive approach to data interpretation in submolecular terms with the additional benefit of their easy implementation [30]. This is why they have been extensively used in the past for the inversion of X-ray and neutron reflectivity data in studies of lipid monolayers at aqueous surfaces [17-19,31-34] or water/oil interfaces [35] as well as protein or polymer interactions with lipid surface layers [13,36-44]. Analogous models for data inversion have also been used to describe molecular layer systems at solid/fluid interfaces [45-51].

Generally, box models can be interpreted in molecular terms. Since the simplest submolecular interpretation of an amphiphilic monolayer structure is a division into a hydrophobic and a hydrophilic



slab, it has naturally been assumed that two boxes are an adequate description of monolayer systems, *c.f.* Fig. 2. The measurement averages over the atomic content of volume elements – located

Figure 2: The layer model – or „box model“ – of lipid surface monolayers, as exemplified with a PC molecule. Averaging over the atomic content of both the hydrophobic slab, containing the chains, and the hydrophilic slab, accommodating the lipid headgroups, leads to homogeneous SLD distributions in these compartments within the monolayer as shown for the electron density at the right. The dashed line indicates the slab structure as it would appear without the broadening of the entire surface film by capillary waves. The broadening is accounted for in the electron density profile indicated by the continuous line.

within these boxes – whose extension is below the resolution limit imposed by the resolution criterion, Eq. (10). Although at first, applications were essentially limited to the determination of layer thickness and SLD values [32,33], it has been recognized early on that an interpretation of the determined SLD values yields information on the molecular organization of the monolayer [28,31]. The SLD ρ_{hphob} of the upper, „hydrophobic“ box is directly related to the lateral density of the alkane chains at the interface – and thus to the area per lipid molecule, A_{lipid} , in the film – if one assumes that no water may interpenetrate into this section of the monolayer:

$$\rho_{hphob} = \frac{n \cdot b_{chain}}{V_{hphob}} = \frac{n \cdot b_{chain}}{A_{lipid} \cdot d_{hphob}} \quad (11a)$$

where n is the number of chains per molecule, b is its scattering length and d the experimentally determined layer thickness. Once the molecular density has been determined, the SLD of the lower box may be accounted for by starting from the assumption – motivated by the chemical structure of the film-forming molecules – that exactly one headgroup is located within the volume $V_{hphil} = A_{lipid} \cdot d_{hphil}$. To fix ρ_{hphil} to the experimentally determined value, n_w water molecules are assumed to hydrate the headgroup, and n_w is determined from the identity,

$$\rho_{hphil} = \frac{b_{hg} + n_w \cdot b_w}{V_{hphil}} \quad (11b).$$

The entire double-layer structure is finally convoluted with a Gaussian, *c.f.* Eq. (8), to account for thermally excited capillary waves that are naturally expected to affect any of the interfaces entering into the box model in the same way. The dependence of their amplitudes on temperature T and surface tension γ has been extensively studied and is quite well understood [52,53]: The parameter σ describing the surface roughness is expected to scale as $\sigma^2 \sim T/\gamma$ [52],* such that with increasing π ($= \gamma_0 - \gamma$) upon film compression, a slight increase in σ is expected. At $\pi \sim 0$ – or clean water surfaces – and room temperature, $\sigma \sim 3 \text{ \AA}$ has been determined.

If one parametrizes chemical models entirely in terms of variables describing the molecular organization – an approach termed „composition-space refinement“ [16] –, one may strictly couple – and thus simultaneously evaluate – data sets from different contrasts, *e.g.*, an X-ray and a neutron data set determined from similarly prepared monolayers of the same chemical entities, or a number of neutron data sets on samples with various isotopic contents [17], thereby increasing the „effective

* An addition constant term, due to the atomic roughness of even an ideally flat surface, is here neglected for the sake of the argument

resolution“ of the experiment considerably [54]. Moreover, one may extract volume information on the submolecular fragments, *e.g.*, for the lipid headgroups by solving

$$V_{hphil} = A_{lipid} \cdot d_{hphil} = V_{hg} + n_w \cdot V_w \quad (12)$$

for the headgroup volume V_{hg} . In doing so, it is usually assumed that the water molecules associated with the headgroups obtain a molecular volume V_w similar to that in bulk water, where $V_w \sim 30 \text{ \AA}^3$.

One frequently used procedure for estimating confidence limits of the determined model parameters is χ^2 mapping [17], in which deviations from the best fit of the model to the experimental data – determined by minimizing

$$\chi^2(\vec{a}) = \frac{1}{N - P} \sum_{i=1}^N \left(\frac{R_i - R(Q_{z,i}, \vec{a})}{\zeta_i} \right)^2 \quad (13),$$

where \vec{a} is a vector in parameter space, R_i is the i th data point with the experimental error bars ζ_i and P are the number of fitted parameters – are quantified by arbitrarily fixing *one* parameter a_i while readjusting all other parameters in \vec{a} to a new (local) minimum. One inherent weakness of this procedure is that a criterion is arbitrarily chosen for the estimate of the confidence limit, such that Δa_i is determined from the value where $\chi^2(\vec{a} \pm \Delta \vec{a}) = (1 + \text{const}) \cdot \chi^2(\vec{a})$ where the constant is of the order of 0.10 ... 0.15.

It is worth while exploring the resolution of reflectivity measurements a bit further, since it has been considerably overestimated occasionally in the past, leading to severe overinterpretation of the data. From neutron reflectivity measurements on DMPC/DMPG mixtures [33] and on various isotopic species of DPPG [34] at the CRISP facility [29] it has been concluded that conformational changes in the glycerol backbone of the respective molecules take place at the monolayer phase transitions, and it has been claimed that the thickness values of the slabs within the monolayer can be determined to a precision of 1 \AA . For good reason, the data presented in the original work do not show error bars – if data are shown at all – and thus Fig. 1 of ref. [33] seems to suggest that the neutron reflectivity measurements contain information in excess of $Q_z = 0.6 \text{ \AA}^{-1}$. More realistically, CRISP produces data from measurements on D_2O – the most favorable subphase compound for floating surface monolayers – out to $Q_z^{\text{max}} \sim 0.25 \text{ \AA}^{-1}$, see, *e.g.*, Fig. 11 of ref. [29], which translates to a canonical resolution of only $\Delta d > 10 \text{ \AA}$, *c.f.* Eq. (10)!

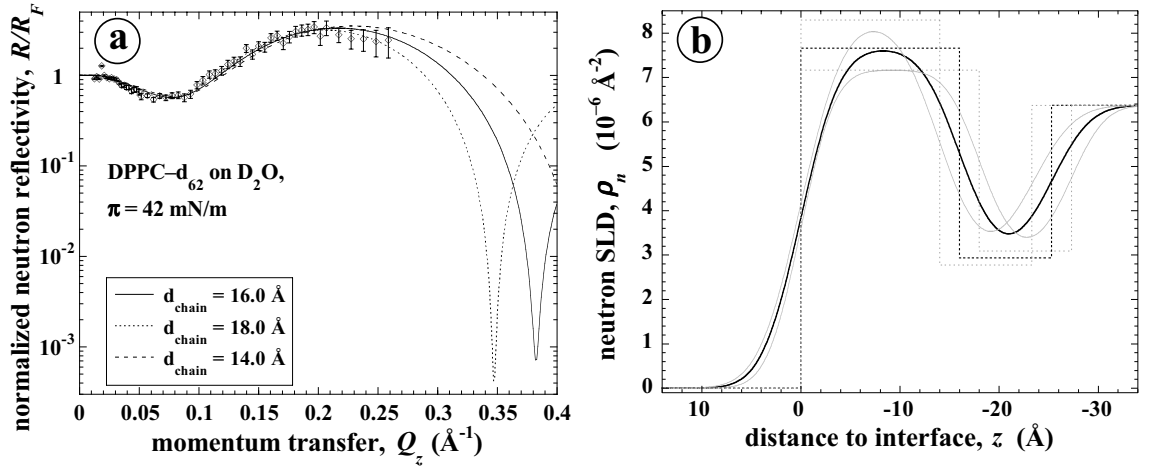


Figure 3: *Qualitative assessment of the information content of a reflectivity data set. Shown in panel (a) is a typical neutron reflectivity data set R/R_F (chain-perdeuterated DPPC- d_{62} on D_2O at $p = 42$ mN/m, c.f. ref. [17]) in comparison with various modeled reflectivities. The continuous line in (a) shows the reflectivity that has been derived from simultaneous refinement of 2 X-ray and 2 neutron data sets, including the one shown in the figure. From this refinement, the hydrophobic layer thickness has been determined to be $d_{\text{hphob}} = 16.0$ Å, and the corresponding SLD profile is shown in panel (b) as a bold line. Detuning of d_{hphob} by ± 2 Å and readjusting the corresponding SLD and the roughness to only fit the DPPC- d_{62}/D_2O data leads to reflectivity models, shown as dashed lines, that cannot be discriminated on account of the experimental data. The corresponding SLD profiles are shown in panel (b) as thin lines. The box structures of the SLD profiles are displayed as broken lines.*

This point can be exemplified by exploring the situation with a similar data set (Figure 3), measured with chain-perdeuterated DPPC- d_{62} on D_2O at the liquid surface reflectometer – then located at TAS7 – of the cold source at the DR3 reactor of Risø National Laboratory (Roskilde, Denmark) [17]. Data have been determined to $Q_z^{\text{max}} \sim 0.25 \text{ Å}^{-1}/R \sim 10^{-6}$ – which is about the best performance of any neutron reflectometer to date. From a simultaneous fitting to X-ray and two different neutron data sets, a layer thickness $d_{\text{hphob}} = 16 \pm 0.6$ Å has been determined [17]. The neutron reflectivity of this model is included in Fig. 3a as a solid line, together with the reflectivities of two other models – dashed lines in Fig. 3a – in which d_{hphob} has been deliberately detuned by ± 2 Å. Subsequently, the corresponding SLD ρ_{hphob} and the roughness σ have been readjusted to a new local χ^2 minimum, while fitting to *only* the singular neutron reflectivity data set (*i.e.*, the headgroup structure remained identical in all three models). As is well perceived from Fig. 3a, *all* three models describe the experimental data reasonably well. A discrimination can only be afforded by measuring the position of the interference minima (right hand side in Fig. 3a), which is out of reach for any neutron reflectivity measurements to date. The associated SLD profiles of the three models are shown in Fig. 3b. Note that the alternate models are *not* limiting cases but rather arbitrarily chosen alternatives. This illustrates that far-reaching conclusions cannot be drawn from *one* single

neutron data set – as not even the hydrophobic slab thickness, although perdeuterated and thus large in its contrast to the other system components, may be determined to any reasonable degree of certainty. This leads to a rule-of-thumb criterion:* The number of boxes in a model that may be determined with certainty from *one* single reflectivity data set equals the number of resolved interference minima, associated with the reflection from the upper and the lower interface of the monolayer (at $Q_z \sim 0.25 \text{ \AA}^{-1}$ in X-ray data, *c.f.* Fig. 1). Cases where such a minimum cannot be experimentally observed encounter similar difficulties as attempts on the determination of structural parameters of monolayers using optical techniques with visible light ($\lambda \gg d_{\text{layer}}$), where only the product ($n_{\text{layer}} \cdot d_{\text{layer}}$) may be determined [55].

On the other hand, the coupling of different contrasts in the composition-space refinement method does lead to an enhanced effective resolution, since it imposes strict conditions on the intervals on which the structural parameters may be varied in the fit, *c.f.* Fig. 3 in ref. [17]. A more rigorous criterion for determining confidence limits of the derived parameters is obtained by fitting the model to „synthetic“ data sets, created by Monte-Carlo sampling that uses the experimental error bars ζ_i as weighting factors [16,54,56,57]. The procedure yields an ensemble of randomly distributed data sets that *could have occurred* given the experimental data and their error bars ζ_i . Fitting of the model to the synthetic data sets – simultaneous fits to simulated data sets from various contrasts or from X-ray and neutron measurements on similarly prepared samples are easily achieved with the composition-space refinement method – then yields a *distribution* of the parameters \vec{a} that results in a realistic description of the confidence limits given the statistical errors of the

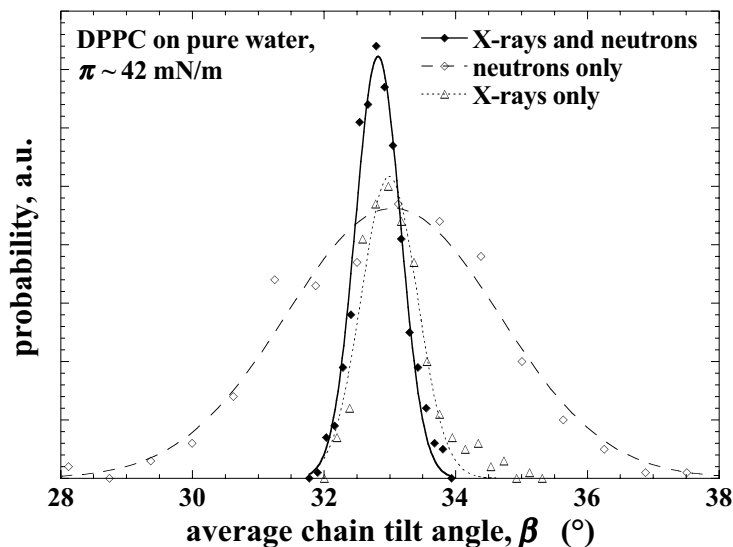


Figure 4: Quantification of the information content of X-ray and neutron reflectivity measurements, exemplified for the average inclination angle of the aliphatic chains, β , in a DPPC monolayer on water. Two different data sets each have been evaluated in the „X-rays only“ (at two different temperatures) and „neutrons only“ (H_2O and D_2O substrates) categories [17]. All four data sets have been evaluated for the „X-rays and neutrons“ category. Probability histograms (16 bins in each distribution) have been derived – for details, see text – that describe confidence levels for the consistency of various values of β with the different X-ray and/or neutron data sets. Since the spread in the β values is different, so are bin widths and thus the integrated probabilities under the continuous lines which are Gaussian fits to the histograms, intended as guides for the eye.

*which might be dubbed „Jens’ criterion“, as it has been frequently advocated by Jens Als-Nielsen as a demand for realistic data evaluation

measurements. For the system discussed above (DPPC at $\pi \sim 42$ mN/m), Fig. 4 shows as an example the distribution of the average chain tilt angle β ($= \arccos(\frac{d_{hphob}}{l_{chain}}$), where $l_{chain} \sim 19.2$ Å is the length of an extended palmitoyl chain) from the surface normal [54]. The lines in the plot indicate Gaussian fits to histograms of the parameter values. The figure shows visually that the simultaneous refinement of progressively more data sets (dashed line: two simultaneously refined neutron data sets; dotted line: two simultaneously refined X-ray data sets; solid line: all four data sets) leads to a better definition of the model parameter β .

One potential problem in the inversion of data at low resolution with box models is a breakdown of the chemical interpretation if the local SLD in the real structure shows large variations along the z direction *within one box*. Whereas such variations cannot be experimentally determined – due to the lack of resolution – they may result in misinterpretations of the atomic contents of the boxes since the interface between them is not naturally determined by chemical composition but rather by the gradients of the SLD, *c.f.* Eq. (9). The steepest gradient within a phospholipid film in which the headgroup extends substantially into the subphase need not be located at the hydrophilic/hydrophobic interface but may occur closer to the phosphate moiety – in which case the chemical interpretation as expressed in Eqns. (11)/(12) might be dangerously misleading. In this context, one may challenge earlier results on the structural reorganization of DMPE and DLPE monolayers [1,19] along the isotherms for which it has been reported that the hydration number, n_w , changes from ~ 24 at $A_{lipid} \sim 80$ Å² to ~ 1.5 for DMPE at 40 Å². At the same time, the interpretation yielded a *decrease* of d_{hphil} upon reduction of A_{lipid} . This would imply a tilting movement of the headgroup dipoles *away* from the surface normal while the average chain directions tilt toward the surface normal upon reduction of the available area per molecule. Moreover, the value of d_{hphil} was invariably close to, or even larger than, the extended length of the PE headgroup. Together with the notion that only 1.5 water molecules should hydrate the phosphate in a compressed monolayer *on top of an infinite reservoir of water* raises severe doubts about the validity of the model. A careful examination of this counterintuitive situation by the authors of that study concluded with the statement that *within the two-box approach* results were robust against variations of details of the model [19].

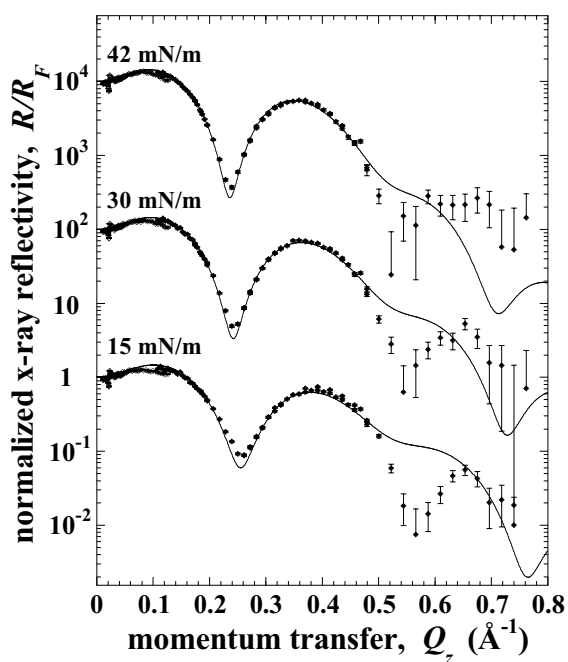


Figure 5: X-ray reflectivity, R/R_F , of DPPC on water at various pressures as indicated. Error bars are due to counting statistics. For clarity, data sets measured at 30 mN/m and 42 mN/m are shifted by factors of 10^2 and 10^4 , respectively. Included are the best fits from a conventional two-box model. While the experimental data are quite well described up to $Q_z \sim 0.5 \text{ \AA}^{-1}$, data and model reflectivities are in serious disagreement beyond 0.5 \AA^{-1} .

The quest for better models and the role of model-free data inversion methods

While problems associated with the molecular interpretation of box-models have been early on recognized, they have nevertheless been frequently used – often without a molecular interpretation – since they are so simple to implement and lead often to a plausible description of the experimental data – at least as long as those were confined to low resolution. In the context of structural investigations of soft condensed matter at interfaces, improvements in synchrotron technology – a boost of the brilliance of the available x-ray intensity by ~ 3 orders of magnitude upon the commissioning of undulator beamlines [11] – were initially utilized to perform more challenging diffraction experiments [12,15]. However, for X-ray reflection experiments on molecular layers at aqueous surfaces, these technical improvements led also to a dramatic development: An increase of the available Q_z range by almost a factor of two (*c.f.* Fig. 1). While trying to exploit this improvement in studies of protein crystallization at phospholipid monolayers, Weygand and coworkers realized [13] that the conventional box models were quite incapable of describing the experimental data at high Q_z – both of the lipid/protein layer system *and* the lipid monolayer prior to protein incubation. To illustrate this point, Fig. 5 shows X-ray reflectivity data of a DPPC monolayer on pure water at three different lateral pressures π , measured at BW1 up to $Q_z^{\max} \sim 0.8 \text{ \AA}^{-1}$, together with the best model descriptions using the conventional two-box approach (solid lines). It is obvious that the data are rather well accounted for up to $Q_z \sim 0.5 \text{ \AA}^{-1}$. However, beyond that, the descriptions are in serious disagreement with the data.* Similar deficiencies of box models have been observed with

*The disagreements in the region of the first interference minima ($Q_z \sim 0.24 \text{ \AA}^{-1}$) are alleviated if one does not attempt fitting the data at $Q_z > 0.5 \text{ \AA}^{-1}$ with the model.

PA [20] and PE [13] lipids such that it seems reasonable to assume that the problems are fundamental in nature.

An analysis of where the description of highly resolved reflectivity data by box models fails has been greatly facilitated by model-free data inversion methods [21,58]. Such techniques permit modeling of reflectivity data with smooth SLD profiles using a set of base functions without making any assumptions about the molecular nature of the underlying system. Out of a multitude of possible solutions that may not be discriminated against each other due to the phase problem, *c.f.* Eqns. (5)/(9), those that are physically most plausible are chosen on a rational basis – typically by suitable constraints to the fit. We have applied the approach by Skov Pedersen and Hamley [22,23] to the highly resolved X-ray reflectivity data from a variety of phospholipids in monolayers to study where differences might occur in the SLD profiles suggested by a model-free and a box-model approach to data inversion.

In brief, the technique uses *b*-splines $B_i(z)$ to describe the SLD distribution across interfaces:

$$\rho(z) = \sum_{i=1}^N a_i B_i(z) \quad (14).$$

N is limited by Q_z^{\max} via the sampling theorem, and the algorithm is constructed as to suppress solutions with large oscillations in ρ by means of a constrained least-squares fit [23]. Details are given in the original work, *c.f.* refs. [21-23].

Using this approach we were able to describe the experimental data satisfactorily up to high Q_z [13]. In most cases studied, discrepancies between the SLD profiles deriving from box-models and the model-free data inversion concerned the headgroup region of the phospholipids, and particularly the interface between the headgroup and the hydrophobic slab within the monolayer: We find this region invariably blurred to a larger extent than expected from a broadening exclusively by capillary waves, *c.f.* Fig. 2a of ref. [13].* Together with the relative heterogeneity of the phospholipid headgroups – as compared to the relatively homogeneous alkane phase – and the well-documented problems of two-box models with a realistic description of these headgroups, this result suggested strongly that better models, particularly for the description of the headgroups in phospholipid monolayers, had to be developed in order to take advantage of the enhanced resolution of synchrotron reflectivity measurements.

*In some cases, the problems of box models at a realistic description of the experimental data is alleviated by using three-box models with *different roughness parameters* σ at all interfaces [13]. In such approaches, however, the aptitude of the box model for a chemical interpretation has been lost.

Volume-restricted distribution function (VRDF) model

By their nature, model-free data inversion techniques do not hint at the chemical composition of the sample, nor do they permit any form of composition-space parameterization which would allow for a simultaneous evaluation of multiple data sets. We have thus developed an alternative description of phospholipid monolayer structures that is based on a composition-space refinement technique and overcomes the obvious deficiencies of the box-modeling approach [20]. The novel data refinement technique is inspired by ideas developed by Wiener and White [16,57,59-61] for the evaluation of X-ray and neutron small angle scattering from planar multi-bilayer systems. In addition, it takes into account recent developments in molecular dynamics simulations of bilayers [24,25], from which volumetric information has been derived and utilized to interpret the small angle scattering data with a higher confidence level.

A realistic scenario describing the structure of phospholipid monolayers should allow for significant conformational changes in the lipid headgroup – *e.g.*, upon going through the monolayer main transition between LE and LC: The headgroup orientation might change from preferentially in-plane – placing the electron-rich phosphate moieties close to the end of the aliphatic chains, into one plane with other headgroup substructures of lower electron density – to preferentially out-of-plane – placing the phosphates into a thin slab of high electron density, separated from the chains by different slabs of lower electron density containing the glycerol backbones and the carbonyls. This structural flexibility is not possible to implement within the framework of a box model, which is the reason why box models are bound to fail at the description of highly resolved data. The real situation is even more complex than the described scenario, which implies that all molecules obtain the same conformation: If the headgroups are disordered along the z axis, *distribution functions* may be the best mode of description.

In their approach to fluid bilayer structure determination, Wiener and White have parsed the lipid molecules into different sections [16] and have modeled the bilayer structure in terms of Gaussian distributions of these fragments [57,60,61]. In a similar procedure, we have introduced a hybrid model that treats the aliphatic chains just as they are accounted for in the box-model approach; the phospholipid backbone and lower headgroup, however, is parsed into fragments that are placed into distribution functions along the interface normal [20]. In distinction from the box model, which satisfies space-filling automatically within the chemical approach to its interpretation, the filling of

space has to be explicitly taken into account in the distribution function approach, since the distribution functions may partially or entirely interpenetrate each other and even if they are separated along z , space-filling is usually not fulfilled at their perimeters. In addition to a satisfactory description of the experimental data, this requires

$$\sum_{\xi} n_{\xi}(z) \cdot V_{\xi} = 1 \quad (15),$$

where $n_{\xi}(z) = \frac{N_{\xi}(z)}{A_{lipid} \cdot dz}$ is the number density of the fragment ξ within the plane located at a distance z from the interface and V_{ξ} is its partial volume. Handling of this additional constraint obviously requires *a priori* knowledge of V_{ξ} or their determination from the fit.

Thermal broadening of the interface structure in the distribution function model derives from two contributions that are well distinguished: A broadening by capillary waves, σ_{cw} , and an intrinsic broadening of fragment positions, σ_{int} , which is the value one would expect to observe *without* capillary waves, *i.e.*, within an interface film at an ideally flat surface. We assume that typical wavelengths for the two processes are well-separated in real space. Hence the upper and lower interfaces of the alkane slab – which we consider atomically flat, at least for the ordered phases LC and SC – are *only* affected by σ_{cw} , whereas the distributions of the headgroups fragments are affected by both contributions which are summed geometrically:

$$\sigma_{total,\xi} = \sqrt{\sigma_{cw}^2 + \sigma_{int,\xi}^2} \quad (16).$$

This separation of the contributions to interfacial broadening permits one both to determine the evolution of intrinsic broadening along the isotherm and to check whether the capillary wave's amplitudes depend on π and T as predicted by theory [53].

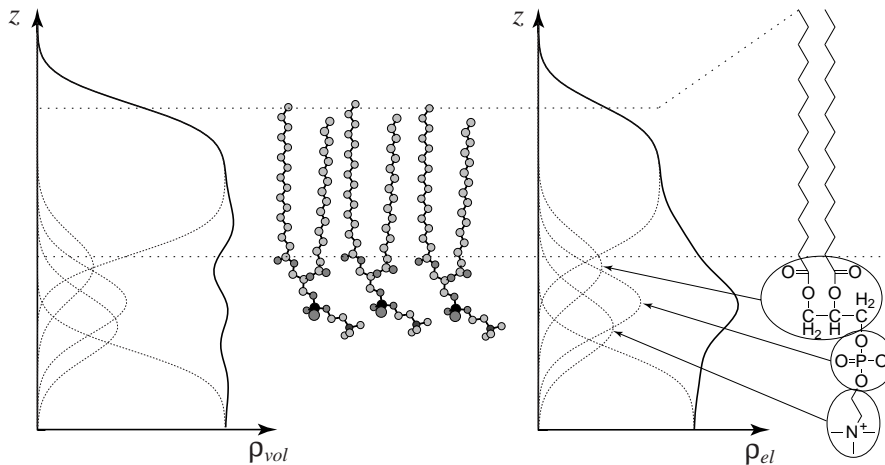


Figure 6: Parsing of phospholipid molecules – shown as an example is DPPC – for modeling in the VRDF approach. Shown is the volume distribution (left), a schematic molecular model of a DPPC monolayer and the resulting electron density distribution together with the molecular structure (right).

Implementation of the VRDF model and performance with DMPA monolayers on water

Figure 6 shows DPPC molecules in a surface monolayer and visualizes the parsing that we have used to model their structure in the distribution function approach to reflectivity data inversion. Also indicated are the electron density profile and the corresponding volume distribution of the substructures (see below). Wiener and White in their evaluation of the fluid DOPC structure in multi-bilayers have parsed the PC headgroups into four substructures [16]: The carbonyls at the lower end of the aliphatic chains, the glycerol backbone, the phosphate, and the terminal cholin moiety. Similarly, the unsaturated chains were treated as a complex series of linked substructures. For structure determination of phospholipids in monomolecular surface layers, we have to be more economic due to a much more restricted information content of the experimental data. If the hydrophobic part of the monolayer is treated in the simplest way imaginable – one homogeneous slab that describes the electron density of the chains –, as is the case for fully saturated alkanes, it is feasible to parse the headgroups into three substructures. We have chosen to treat the carbonyls and glycerol as one (GC) substructure and the electron-rich phosphate as another one (P), leaving whatever follows at the terminal end of the headgroup in different phospholipids as the third substructure. If one chooses to study cation binding from the subphase to the headgroup – as we have done in the original work reported here (see below) –, the bound ions may be formally treated as yet another (Cat) substructure in the system. Any of these headgroup substructures may be associated with an arbitrary number of water molecules – to be determined from the fit or guessed from chemical considerations – which together with the respective headgroup component determines the scattering length density and volume contributions of that moiety.

We have used an efficient algorithm deriving from the Parratt formalism [30] to compute model reflectivities based on SLD profiles that follow from the fragment distribution in space [20]: (1) The hydrophobic part of the monolayer is treated as a genuine box in the spirit of Parratt’s approach with a global roughness parameter σ_{cw} , due to capillary waves, which broadens both the upper and the lower interfaces in space. (2) The headgroup fragments are formally treated as boxes as well, albeit with an unphysically narrow width ($\Delta z = 1.5 \text{ \AA}$) and large SLD, ρ_{box} , but the correct scattering length (per unit area), $b / A_{lipid} = \rho_{box} \cdot \Delta z$ [20]. These “dummy boxes” are centered at the centers of the respective fragment distributions with no scattering length in between, such that the correct scattering length (per unit area) is obtained by integrating over the box structure along the

interface normal. The headgroup boxes are then smeared into a series of error functions with $\sigma_{\text{erf}} = \sigma_{\text{total},\xi}$, c.f. Eq. (16), incorporating contributions from both the capillary waves and the intrinsic broadening, specific for the fragment ξ . Since $2\sigma_{\text{erf}} \gg \Delta z$, this leads to a proper representation of the SLD profile, as the broadened boxes are virtually indistinguishable from genuine Gaussian distributions. In fact, we observed that discrepancies of the reflectivities derived from this approach with those computed from SLD profiles that were implemented as a large number of thin slabs – which are, however, much more tedious to treat numerically – were always $< 3\%$.

We have used volumetric information derived from molecular dynamics simulations [25] to implement constraints to the electron density distributions by requiring that space filling in the headgroup region of the monolayer be optimized *together* with minimizing the deviations between model reflectivity and experimental data [20]. This is formally implemented as an extension to Eq. (13) which is based on Eq. (15):

$$\chi'^2 = \chi^2 + e^{DX} \quad (17)$$

with a weighting factor D – chosen to be $D = 800$ in the work reported below – and

$$X = \frac{1}{N} \sum_{i=1}^N \left(\sum_{\xi} n_{\xi}(z_i) V_{\xi} - 1 \right)^2 \quad (18).$$

In earlier work on DMPA monolayers, we have shown that the GC and P fragment volumes given by Armen et al. [25], $V_{GC} = 146.8 \text{ \AA}^3$ and $V_P = 53.7 \text{ \AA}^3$, are consistent with values derived from the fit [20] – where it has to be taken with a grain of salt that these results are quite „soft“, as a large number of free parameters were fitted for such a comparison.

In a first application of the VDRF model, the structure of DMPA in monolayers on pure water has been determined from X-ray reflectivity at five pressure values π along the isotherm [20]. Using the constraints imposed by the chemical structure, the position of the GC fragment was strictly coupled to the ends of the alkane chains. The broadening of the headgroup fragments was assumed to be equal in the implementation of the new model in that work. Moreover, since a more sophisticated implementation of the model had suggested that the GC fragment is essentially water-free within the resolution of the method, no water was assumed located at GC [20].

From the X-ray reflection measurements it was deduced [20] that both the average chain tilt angle β and the average headgroup tilt angle α – evaluated as the direction of the vector pointing from the center-of-mass of the GC fragment to the phosphate – decrease significantly across the

main phase transition (LE \rightarrow LC), although the changes in α are surprisingly low ($\alpha \sim 65^\circ$ in LE and $\sim 48^\circ$ in LC). Even more surprising was the observation that the hydration of the phosphate stays essentially constant along the isotherm ($n_p^w \sim 6$ in LE and ~ 5 in LC). The latter is in disagreement with earlier X-ray reflectivity work on PE monolayers in which by using a two-box model it was determined that the change in headgroup hydration is large ($n_{hg}^w \sim 24 \dots 14$ in LE and ~ 1.5 in LC). The global interface roughness parameter σ_{cw} was observed to increase from values $< 3 \text{ \AA}$ at $\pi < 15 \text{ mN/m}$ to $\sim 3.5 \text{ \AA}$ at 45 mN/m . * $\sigma_{int,P} \sim 1.4 \dots 2.2 \text{ \AA}$ ($\pi = 2 \dots 45 \text{ mN/m}$) was always significantly larger than zero and was observed to increase monotonously with π [20].

RESULTS AND DISCUSSION: DMPA ON SUBPHASES CONTAINING DIVALENT CATIONS

We have used the VDRF model as outlined in the previous section to study ion binding to DMPA monolayers. Partial volumes of the ions have been estimated from their radii and taken to be $V_{Ca^{2+}} = 4 \text{ \AA}^3$, $V_{Ba^{2+}} = 10 \text{ \AA}^3$ and $V_{Cl^-} = 25 \text{ \AA}^3$. Figure 7a shows X-ray reflectivity data, R/R_F , of a DMPA monolayer on 10 mM BaCl_2 at $\pi = 4 \text{ mN/m}$, $T \sim 22^\circ\text{C}$ together with various model fits. Upon applying the general approach to modeling the lipid structure in the presence of cations we found that one cannot simply assume a stoichiometric, $2 : 1$ (DMPA $^-$: Cat $^{2+}$), ratio. Instead, the number of ions included in the headgroup has to be determined from the fit. On the other hand, we observed that the position of the bound cations along the surface normal coincides with the position of the phosphate, such that one may model the P and Cat fragments using *one* distribution function along the z axis. As a practical consequence, one may then directly determine the overall number of water molecules in the headgroup without having to make any assumption on a specific association ratio, water : cation. Moreover, this result implies that cations are either firmly bound in the headgroup or dissociated: We do not observe a cloud of charge close to the monolayer within the resolution of the experiment.

Surprisingly for us, we found that the extra scattering length of the bound ions in the headgroup does not amount to $\Delta n_{hg}^e = 27$, *i.e.*, half the number of electrons of the Ba $^{2+}$ ion, as would be expected for stoichiometric binding. The dotted line in Fig. 7a shows the best fit obtained with the assumption of a $2 : 1$ DMPA $^-$: Ba $^{2+}$ ratio. The model is clearly inadequate of describing the

*In the LE phase slightly larger σ_{cw} values were observed, presumably indicative of a roughening of the alkane/air interface due to atomic roughness of the chain ends that is not accounted for by the model [20].

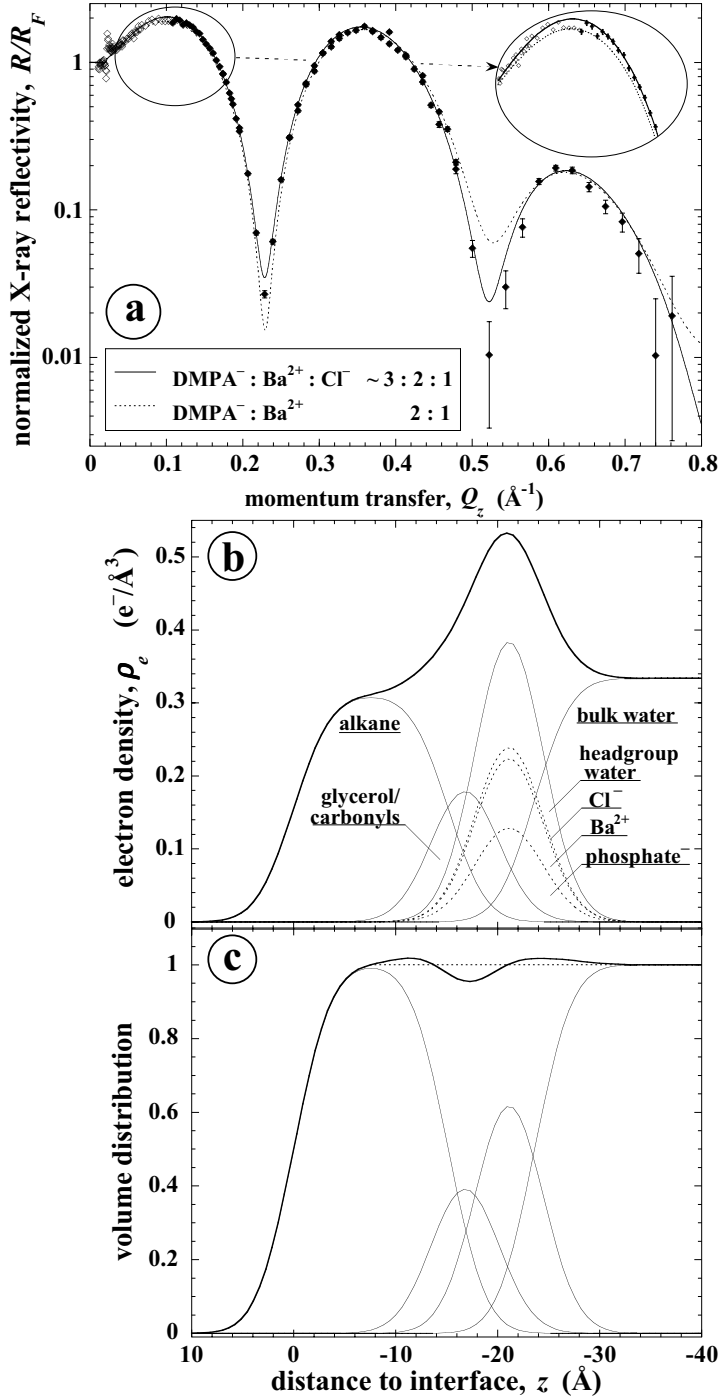


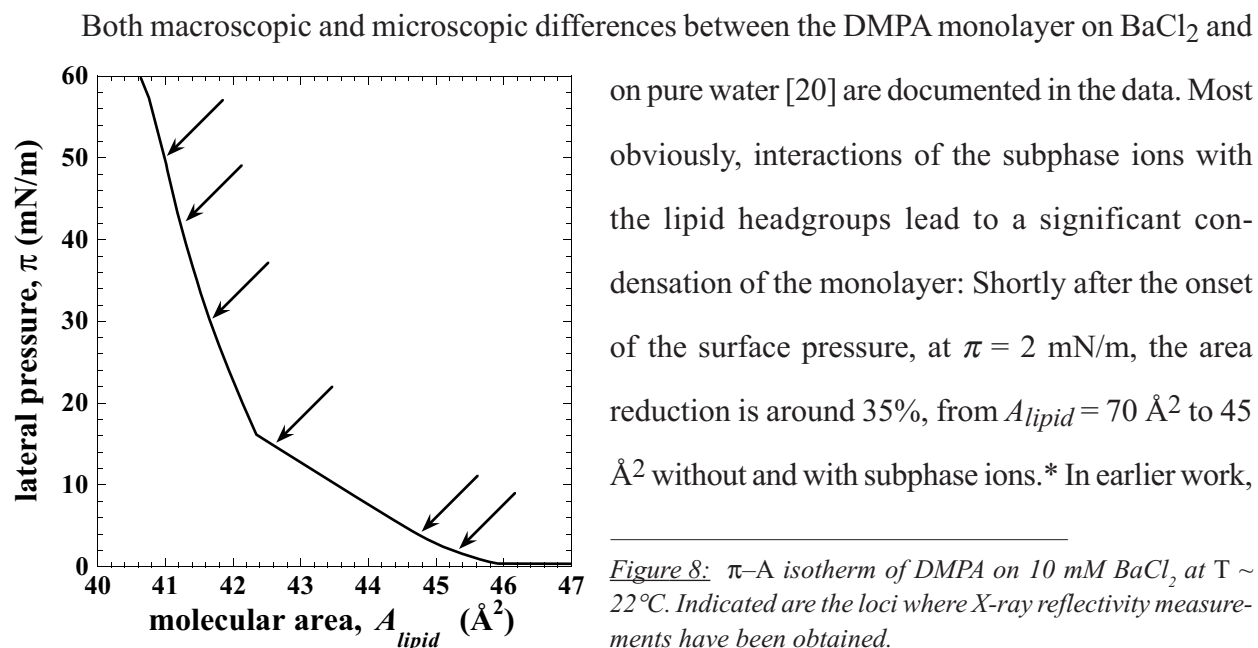
Figure 7: (a) High resolution X-ray reflectivity data, R/R_F , of a DMPA monolayer on 10 mM BaCl_2 at $\pi = 4 \text{ mN/m}$ in comparison with the reflectivities computed for two different models. Dotted line: Best fit for a stoichiometric binding model ($0.5 \text{ Ba}^{2+} : \text{DMPA}$) within the distribution function approach: $\chi^2 \sim 18.4$. Continuous line: VRDF model that allows for binding of Ba^{2+} and Cl^- to the P-fragment within the headgroup under the assumption of charge neutralization (best fit parameters are summarized in Table 1, $\chi^2 \sim 3.1$). The inset in the upper right corner shows a close-up comparison between the data and the competing models at low Q_z .

(b) Electron density distribution and (c) volume distribution across the interface derived from the X-ray reflectivity shown in (a) using the distribution function model that allows for simultaneous binding of Ba^{2+} and Cl^- to the phosphate. The envelopes are shown in bold lines and the component contributions in thin lines. In panel (b), the electron density distribution at the phosphate position is broken down in the partial contributions of the (dry) phosphate, cations, anions, and bound water. In panel (c), deviations from unity at $z < -8 \text{ \AA}$ (dotted line) occur as a compromise between the requirements of optimal modeling of the experimental X-ray data and optimized volume filling, c.f. Eqns. (13), (17) and (18).

experimental data satisfactorily. An assumption of increased amounts of water in the headgroup even deteriorates the fit to the data: The electron density in the headgroup region is *larger* – not lower – than a stoichiometric model would suggest. On the other hand, overcompensation by Ba^{2+} ions would leave the interface positively charged – a rather unlikely scenario for a monolayer on an infinite reservoir of ions of *both* charges! We conclude that the most realistic description of the monolayer at low π /large A_{lipid} is one with *both*, Ba^{2+} and Cl^- , ion species included in the lipid headgroups. We have thus assumed in the modeling described below that two mobile charged species, Ba^{2+} and BaCl^+ – accounted for by the same distribution function which is also used for the headgroup fragments –, contribute to the electron density in the headgroup region. The electron density profile derived from the best fit based on this assumption, shown in Fig. 7b, leads to a satisfactory description of the experimental

data – included as a solid line in Fig. 7a – and reduces the χ^2 value of the fit from ~ 18.4 to ~ 3.1 while space filling is also reasonably well achieved ($X \sim 2 \times 10^{-4}$), *c.f.* Fig. 7c. Moreover, all the remaining structural parameters describing the monolayer attain physically reasonable values and fall in line with a consistent development upon compression of the monolayer along the isotherm (see below). We thus conclude that the proposed model represents the most plausible description of the monolayer on an ionic subphase.

Figure 8 shows the isotherm ($T = 22 \pm 0.5^\circ\text{C}$) of DMPA on 10 mM BaCl_2 . In the expanded regime, $A_{lipid} > 42 \text{ \AA}^2$, it is characterized by a slow continuous rise of π upon compression with no clear signature of a fluid/gel phase transition. Beyond $\pi \sim 15 \text{ mN/m}$, the compressibility decreases discontinuously which indicates that the monolayer has adopted a highly condensed phase state. X-ray reflectivities have been determined in the regime of high compressibility ($\pi = 2 \text{ mN/m}$ and 4 mN/m), near the turning point ($\pi = 15 \text{ mN/m}$), and in the regime of low compressibility ($\pi = 30 \text{ mN/m}$, 42 mN/m and 50 mN/m). The experimental data together with optimized distribution function models (continuous lines) are displayed in Fig. 9, and the corresponding best-fit parameter values are summarized in Table 1. To illustrate the sensitivity of the model to changes of the optimized parameter sets and to estimate confidence levels, χ^2 mapping [17,20] has been performed. Some of the maps relating to the monolayer at 4 mN/m – for those parameters that we consider most important in this work and will discuss extensively in what follows – are shown in Fig. 10. As earlier [20], an increase of χ^2 of 10% over the minimum has been defined as the criterion to determine the confidence limits on the optimized parameters.



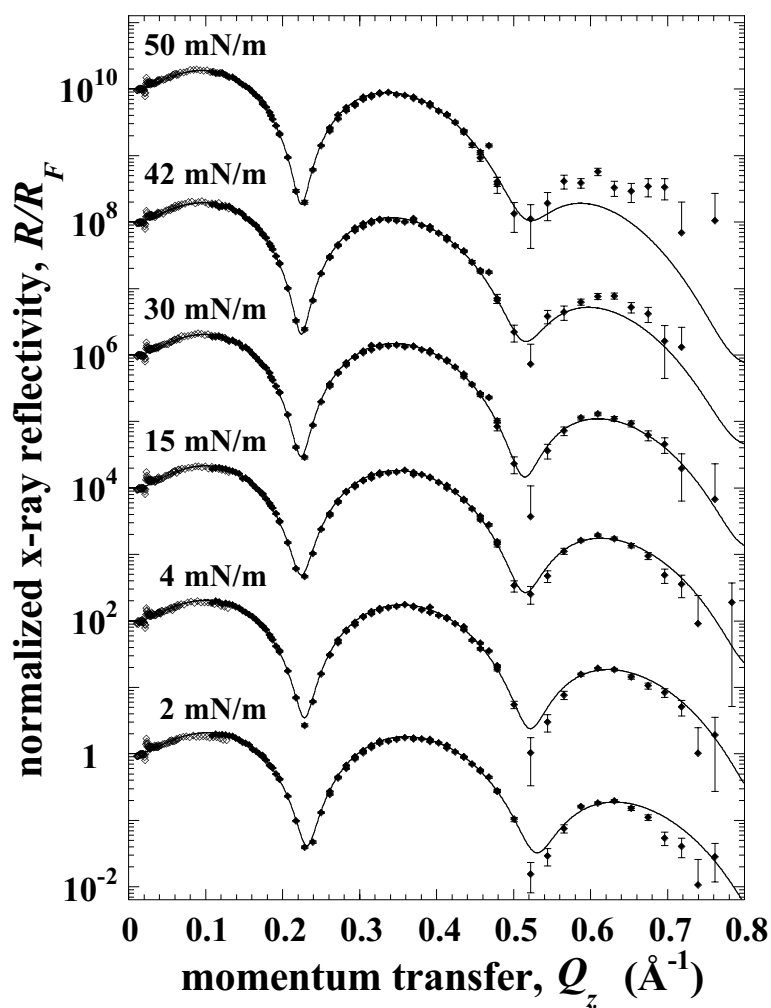


Figure 9: X-ray reflectivity, R/R_F , of DMPA on 10 mM BaCl_2 at $T \sim 22^\circ\text{C}$. Error bars are due to counting statistics. For clarity, successive data sets have been shifted by factors of 100 and some of the error bars in the negative direction have been omitted. Solid lines are best fits of the distribution function models allowing for simultaneous binding of cations and anions to the headgroup. The relevant parameter values are listed in Table 1.

it has been assumed that the compact, highly charged divalent cations determine entirely the changes in the isotherms [62] since binding of anions was considered unlikely at all surface densities of the lipid because a large reduction of the anion concentration close to the negatively charged interface from the bulk value is expected [63]. The most notable result

from the work reported here is that this view has to be revoked in parts in that at large A_{lipid} a significant amount of anions is observed in the lipid headgroups, at least at the high salt conditions that we have investigated.

The density of the alkane phase is essentially constant along the isotherm until the formation of the condensed phase is completed at $\pi \sim 15$ mN/m – a continuous tilting of the chains toward the surface normal accommodates for the reduction in available area –, and increases slightly as π rises to 30 mN/m and beyond while surplus Ba^{2+} and Cl^- ions are squeezed out of the headgroup. This is similar to the behavior observed with DMPA on pure water for which it has been observed [20] that the available area A_{lipid} controls the average chain tilt angle, β , with the notable difference that the change of A_{lipid} – and hence the change of β – is much larger for DMPA on water than in the monolayer on BaCl_2 .

It is not surprising that the most pronounced differences between the DMPA monolayers on

*It should be noted that the investigation of DMPA on pure water has been performed at slightly elevated temperatures, $T \sim 27^\circ\text{C}$ [20].

lateral pressure	π (mN/m)	2	4	15	30	42	50	
area per molecule	A_{lipid} (\AA^2)	45.2	44.7	42.7	41.7	41.3	41.0	constant
chain slab thickness	d_{chain} (\AA)	14.9	15.2	15.7	16.1	16.0	15.9	parameter
average chain tilt angle	β (deg.)	27	25	20	15	16	17	dependent variable
GC position	z_{GC} (\AA)	-16.5	-16.8	-17.4	-17.9	-17.8	-17.7	dependent variable
P position	z_P (\AA)	-20.7	-21.1	-21.7	-22.0	-22.1	-21.9	parameter
projected GC–P distance	d_{GC-P} (\AA)	4.2	4.3	4.3	4.2	4.3	4.2	dependent variable
average headgroup orientation angle	α (deg.)	37	35	36	38	36	37	dependent variable
global interface roughness	σ_{cw} (\AA)	2.9	2.9	3.0	3.2	3.6	4.0	parameter
internal fragment distribution width	σ_{int} (\AA)	1.5	1.7	1.8	1.9	1.6	1.2	parameter
total width of distribution function	σ_{total} (\AA)	3.3	3.4	3.5	3.7	3.9	4.2	dependent variable
Ba ²⁺ per DMPA ⁻	n_p^{Ba}	0.675	0.66	0.69	0.605	0.53	0.50	parameter
Cl ⁻ per DMPA ⁻	n_p^{Cl}	0.35	0.32	0.38	0.21	0.06	0.0	dependent variable
water molecules per headgroup	n_p^W	5.0	5.4	5.4	5.8	6.0	5.2	parameter

Table 1: Structural parameters describing DMPA molecules in a Langmuir monolayer on an aqueous solution of 10 mM BaCl₂, as derived from composition-space refinement of X-ray reflectivity data. For the component volumes, values from molecular simulations [25], $V_{GC} = 146.8 \text{ \AA}^3$ and $V_p = 53.7 \text{ \AA}^3$, have been assumed. The extended lengths of the myristoyl chains, $l_{chain} = 16.7 \text{ \AA}$, and the distance between the center-of-gravity of the GC fragment and the phosphate in an extended configuration, $l_{GC-P} = 5.27 \text{ \AA}$, have been estimated from a MM2-optimized molecular model. Partial ion volumes have been assumed to be $V_{Ba^{2+}} = 10 \text{ \AA}^3$ and $V_{Cl^-} = 25 \text{ \AA}^3$. Dependent variables have been computed using a higher numerical precision of the independent parameters than that shown.

water and on BaCl₂ concern the behavior of the lipid’s headgroup. Whereas on pure water the mean orientation angle of the headgroup, α , has been reported to follow the development of β across the LE/LC phase transition [20], in the monolayer on BaCl₂ it is independent of π in the entire range between 2 mN/m and 50 mN/m – and of much smaller value, indicating that the headgroup extends more toward the aqueous phase in the presence of ions. Nevertheless, the overall composition and hence the molecular organization of the headgroup region changes a lot: At low π , cation binding to the charged DMPA headgroup leads to charge overcompensation, which is in turn compensated for by the binding of Cl⁻ from the subphase. This leads to a strong accumulation of electron density within the headgroup which is sensitively detected in the X-ray experiments. Upon increasing π , this situation gradually changes toward the state of stoichiometric binding of cations by the PA

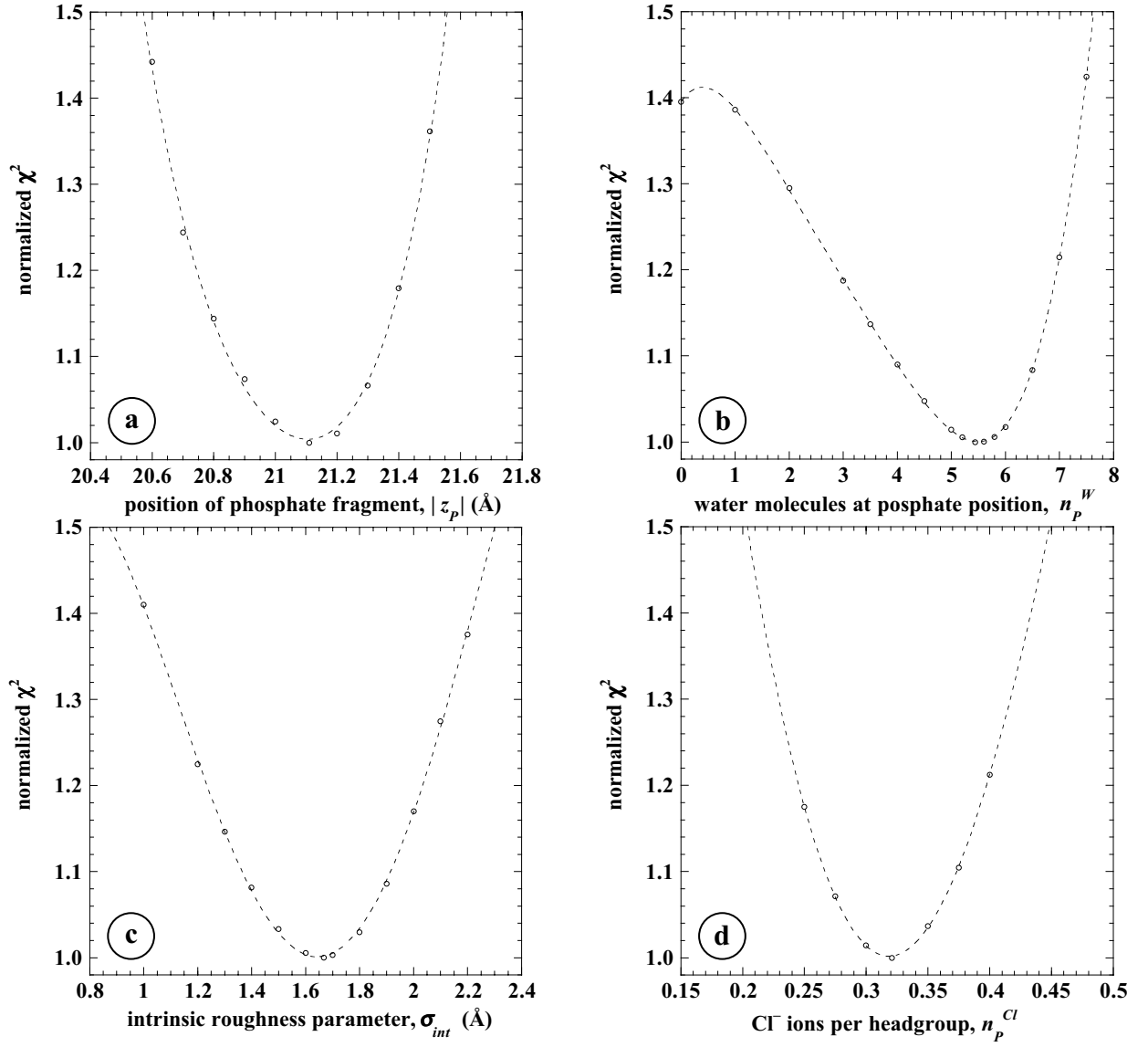


Figure 10: Results on selected parameters from the χ^2 mapping of fits obtained from the VRDF approach to modeling the DMPA monolayer on 10 mM BaCl_2 at 4 mN/m that allows for simultaneous binding of cations and anions. For the determination of confidence levels on the model parameters, an increase of the χ^2 value of 10% above its minimum has been taken as a criterion. Dotted lines are guides for the eye.

headgroup, which is, however, only approached at lateral pressures beyond 40 mN/m. In fact, only for the measurement at the highest value of π , 50 mN/m, that has been performed we find that the stoichiometric ratio is exactly attained. As observed with DMPA monolayers on pure water, the hydration number is constant over the entire range of surface pressures, $n_p^W = 5 \dots 6$. Particularly, we find no indication that the increased amount of ions incorporated into the headgroup at low π leads to an increase of the number of water molecules, suggesting that phosphate, anions and cations form a tightly bound complex within the headgroups in which water molecules play a minor role, if any.

The global interface broadening σ_{cw} due to capillary waves behaves qualitatively as expected from theory [53] and is consistent with the behavior observed in earlier work [20]: It raises gradually upon increasing π —*i.e.*, decreasing surface tension γ —and falls within 0.1 Å of the values determined

in ref. [20] at the respective π values. At the lowest π values for the DMPA monolayer on pure water an anomalous increase of σ_{cw} has been observed, which was attributed to a contribution of atomic roughness of the disordered chains in the LE phase to the value of the parameter σ_{cw} [20] because such an atomic roughening is not accounted for in the simple model. With DMPA on ionic subphase, such an increase of σ_{cw} is not observed – $\sigma_{cw} < 3.0 \text{ \AA}$ at all $\pi < 15 \text{ mN/m}$ –, which corroborates our interpretation of the DMPA structure on pure water and indicates that the low pressure phases are distinct in the two experimental situations. Up to $\pi = 30 \text{ mN/m}$, the internal fragment distribution width σ_{int} , characterizing also the distribution of the cations and anions, develops exactly like headgroup fragment distribution width of DMPA on pure water, *c.f.* Table 1 in ref. [20], not only qualitatively but also quantitatively to within 0.1 \AA . While this agreement to a fraction of 1 \AA may be fortuitous, the general observation confirms our confidence that the parameterization of the model is valid. In sharp contrast to the gradual increase of σ_{int} upon compression, a drop is observed above $\pi = 30 \text{ mN/m}$, in a regime of the isotherm where both the compressibility and $A_{lipid} \sim 41 \text{ \AA}^2$ are already quite low – and the latter approaches the limiting area of $\sim 40 \text{ \AA}^2$ for two aliphatic chains in the crystalline state, as determined from GIXD [10]. It is tempting to speculate that this reduction in σ_{int} may be the signature of a pressure-induced ordering of the phospholipid headgroups. One should, however, keep in mind that the reliability of the parameter σ_{int} is low at high π , since σ_{cw} is large and σ_{int} is contained in a quadratic sum that yields σ_{total} , *c.f.*, Eq. (16), *i.e.*, the quantity that is directly determined from the properties of the model-derived electron density distribution.

We have also measured the X-ray reflectivity of a DMPA monolayer on a subphase of 10 mM CaCl_2 at $\pi = 5, 10, 30,$ and 40 mN/m ($T = 27^\circ\text{C}$; data not shown) and have evaluated the results using the same formalism [64]. While the reliability of the derived parameters is inferior to that obtained with DMPA on BaCl_2 due to the reduced contrast in the electron density profiles of the monolayer, the general picture is quite similar to the one developed above. Particularly, we find that both cations and anions must be involved to model the reflectivities satisfactorily. For similar areas A_{lipid} we observe identical Cl^- concentrations – within a few percent – in the DMPA headgroup on CaCl_2 and on BaCl_2 subphases. Since A_{lipid} at the largest pressure π for which the reflectivity has been determined on the CaCl_2 subphase – $A_{lipid} \sim 42.3 \text{ \AA}^2$ – is significantly larger than $A_{lipid} \sim 41.0 \text{ \AA}^2$ for the DMPA monolayer on BaCl_2 at 50 mN/m , we never observed the situation of stoichiometric binding of $\text{Ca}^{2+} : \text{DMPA}^-$. At $\pi = 40 \text{ mN/m}/42.4 \text{ \AA}^2$, a ratio of $\sim 0.30 \text{ CaCl}^+$ per

DMPA⁻ falls in line with the observation of ~ 0.38 BaCl⁺ per DMPA⁻ at $\pi = 15$ mN/m/42.7 Å² and ~ 0.21 BaCl⁺ per DMPA⁻ at $\pi = 30$ mN/m/41.7 Å². Due to the higher temperature, resulting in larger A_{lipid} , the headgroup orientation is slightly more coplanar in the experiment with CaCl₂ subphase as compared with the BaCl₂ case. We observed parameter values that scattered around $\alpha = 40$ within $\pm 3^\circ$ for all π values that correspond to a variation of A_{lipid} between 46.7 and 42.3 Å².

CONCLUSIONS

Reflectivity measurements, both using X-ray or neutron radiation, constitute a powerful tool to determine the submolecular structures of organic molecular interface layers at solid substrates as well as on the surface of liquids. Particularly valuable is their capability for the characterization of *disordered* systems, at which surface sensitive diffraction methods are bound to fail. In the context of biophysical chemistry, the structural organization of phospholipid monolayers is of high relevance for the comprehension of biomembrane interfaces. In the past, box models have been used to unveil information contained in reflectivity measurements particularly of insoluble organic monolayers on water surfaces. They have been proven to be both valuable and adequate as long as momentum transfer ranges up to $Q_z \sim 0.5$ Å⁻¹ were involved. Specifically on the hydrophobic alkane slabs within such molecular layers, detailed information has been obtained using this data inversion method. However, not always has the interpretation of experimental data been based on a realistic estimate of their information content. Particularly neutron reflectivity data, which are generally restricted to a quite narrow momentum transfer range, have been overinterpreted in the past. Only the joint refinement of neutron data from various contrasts, *e.g.*, in a composition-space parameterization of the models used for data inversion, make neutron reflectivity data worth the effort of their collection.

A development that is recently boosting the field is based on technical improvements of synchrotron and laboratory X-ray sources which have extended the available Q_z range considerably. This has in turn stimulated the development of more sophisticated molecular models for data inversion, particularly as it has been shown that conventional box models are no longer adequate descriptions if Q_z values of up to 0.8 Å⁻¹ are involved. The simultaneous development of molecular simulations of biomembranes – from which volumetric information has been derived – has greatly facilitated the application of the composition-space refinement, introduced to the data inversion using box models a few years ago [17], in a distribution function approach to modeling the molecular

structure of the headgroups within phospholipid monolayers at the air/water interface. In a first application, we have used this new approach for the determination of the submolecular structure of DMPA monolayers, thereby revealing a wealth of new structural information. For the first time we were recently able to extract detailed – and plausible – information on the organization of lipid headgroups and its response to the main monolayer phase transition, LE \rightarrow LC. In contradiction to earlier interpretations of X-ray reflectivity data in a more limited Q_z range we observe that the hydration of the phosphate does not significantly change across the phase transition and, more generally, along the isotherm. This result is corroborated by a similar observation with DMPA monolayers in the presence of divalent cations, reported in this work. Here, the sensitivity of the method is so high – due to the extraordinarily large electron density of the Ba²⁺ ion – that the composition of the headgroup can be analyzed in detail, revealing charge overcompensation by Ba²⁺ which results in the incorporation of anions along with the cations.

A next step on the way to investigate more physiologically relevant systems will include analyses of more complicated headgroup structures in complex phospholipids, the intercalation of small molecular compounds into such structures or the biospecific adsorption of proteins. Inevitably, as the number of model parameters increases, data will be more difficult to interpret quantitatively. However, with the powerful tool of composition-space refinement at hand, a joint refinement of X-ray and neutron data within the distribution function approach is straightforward and may pave the way for the determination of complex structures that we have not even dared to dream about in monolayer research until recently.

ACKNOWLEDGMENTS

We thank Kristian Kjaer (Risø National Laboratory, Roskilde, Denmark) for his devising of the liquid surface experimental station at BW1 and valuable advise for the experimental work, as well as Markus Weygand and Peter Krüger for help with the measurements. We acknowledge beam time at HASYLAB (DESY, Hamburg, Germany) under project no. II-97-51. The work has been financially supported by the DFG through the SFB 294 (TP F3) and by the Fonds der Chemischen Industrie (Frankfurt, Germany).

REFERENCES

- [1] H. Möhwald, *Annu. Rev. Phys. Chem.* 41 (1990) 441.
- [2] H.M. McConnell, *Annu. Rev. Phys. Chem.* 42 (1991) 171.
- [3] C.M. Knobler and R.C. Desai, *Annu. Rev. Phys. Chem.* 43 (1992) 207.
- [4] J. Als-Nielsen and H. Möhwald, In *Handbook on Synchrotron Radiation*, S. Ebashi, M. Koch and E. Rubinstein (Eds.), Elsevier North-Holland, Amsterdam 1991, 1.
- [5] J. Als-Nielsen, D. Jacquemain, K. Kjaer, M. Lahav, F. Leveiller and L. Leiserowitz, *Phys. Rep.* 246 (1994) 251.
- [6] I. Weissbuch, R. Popovitz-Biro, M. Lahav, L. Leiserowitz, K. Kjaer and J. Als-Nielsen, In *Adv. Chem. Phys.*, I. Prigogine and S.A. Rice (Eds.), Wiley, New York 1997, 39.
- [7] K. Kjaer, J. Als-Nielsen, C.A. Helm, L.A. Laxhuber and H. Möhwald, *Phys. Rev. Letters* 58 (1987) 2224.
- [8] P. Dutta, J.B. Peng, B. Lin, J.B. Ketterson, M. Prakash, P. Georgopoulos and S. Ehrlich, *Phys. Rev. Letters* 58 (1987) 2228.
- [9] V.M. Kaganer, G. Brezesinski, H. Möhwald, P.B. Howes and K. Kjaer, *Phys. Rev. Letters* 81 (1998) 5864.
- [10] V.M. Kaganer, H. Möhwald and P. Dutta, *Rev. Mod. Phys.* 71 (1999) 779.
- [11] R. Frahm, J. Weigelt, G. Meyer and G. Materlik, *Rev. Sci. Instrum.* 66 (1995) 1677.
- [12] H. Haas, G. Brezesinski and H. Möhwald, *Biophys. J.* 68 (1995) 312.
- [13] M. Weygand, B. Wetzer, D. Pum, U.B. Sleytr, K. Kjaer, P.B. Howes and M. Lösche, *Biophys. J.* 76 (1999) 458.
- [14] M. Weygand, M. Schalke, P.B. Howes, K. Kjaer, J. Friedmann, B. Wetzer, D. Pum, U.B. Sleytr and M. Lösche, *J. Mater. Chem.* 10 (2000) 141.
- [15] S.A.W. Verclas, P.B. Howes, K. Kjaer, A. Wurlitzer, M. Weygand, G. Büldt, N.A. Dencher and M. Lösche, *J. Mol. Biol.* 287 (1999) 837.
- [16] M.C. Wiener and S.H. White, *Biophys. J.* 59 (1991) 174.
- [17] D. Vaknin, K. Kjaer, J. Als-Nielsen and M. Lösche, *Biophys. J.* 59 (1991) 1325.
- [18] C.A. Helm, H. Möhwald, K. Kjaer and J. Als-Nielsen, *Europhys. Lett.* 4 (1987) 697.
- [19] C.A. Helm, P. Tippmann-Krayer, H. Möhwald, J. Als-Nielsen and K. Kjaer, *Biophys. J.* 60 (1991) 1457.

- [20] M. Schalke, P. Krüger, M. Weygand and M. Lösche, *Biochim. Biophys. Acta* 1464 (2000) 113.
- [21] J. Skov Pedersen and I.W. Hamley, *Physica B* 198 (1994) 16.
- [22] I.W. Hamley and J. Skov Pedersen, *J. Appl. Cryst.* 27 (1994) 29.
- [23] J. Skov Pedersen and I.W. Hamley, *J. Appl. Cryst.* 27 (1994) 36.
- [24] H.I. Petrache, S.E. Feller and J.F. Nagle, *Biophys. J.* 70 (1997) 2237.
- [25] R.S. Armen, O.D. Uitto and S.E. Feller, *Biophys. J.* 75 (1998) 734.
- [26] D.A. Cadenhead, F. Müller-Landau and B.M.J. Kellner, In *Ordering in Two Dimensions*, S.K. Sinha (Eds.), Elsevier North Holland, Amsterdam 1980, 73.
- [27] P. Krüger, M. Schalke, J. Linderholm and M. Lösche, *Rev. Sci. Instrum* (2000) submitted.
- [28] J. Als-Nielsen and K. Kjaer, In *Phase Transitions in Soft Condensed Matter*, T. Riste and D. Sherrington (Eds.), Plenum Press, New York 1989, 113.
- [29] J. Penfold and R.K. Thomas, *J. Phys.: Condens. Matter* 2 (1990) 1369.
- [30] L.G. Parratt, *Phys. Rev.* 95 (1954) 359.
- [31] K. Kjaer, J. Als-Nielsen, C.A. Helm, P. Tippmann-Krayer and H. Möhwald, *J. Phys. Chem.* 93 (1989) 3200.
- [32] M.J. Grundy, R.M. Richardson, S.J. Roser, J. Penfold and R.C. Ward, *Thin Solid Films* 159 (1988) 43.
- [33] T.M. Bayerl, R.K. Thomas, J. Penfold, A. Rennie and E. Sackmann, *Biophys. J.* 57 (1990) 1095.
- [34] T. Brumm, C.T. Naumann, A.R. Rennie, R.K. Thomas, D. Kanellas, J. Penfold and T.M. Bayerl, *Eur. Biophys. J.* 23 (1994) 289.
- [35] M. Thoma, M. Schwendler, H. Baltes, C.A. Helm, T. Pfohl, H. Riegler and H. Möhwald, *Langmuir* 12 (1996) 1722.
- [36] S.J. Johnson, T.M. Bayerl, W. Weihs, H. Noack, J. Penfold, R.K. Thomas, D. Kanellas, A.R. Rennie and E. Sackmann, *Biophys. J.* 60 (1991) 1017.
- [37] D. Vaknin, J. Als-Nielsen, M. Piepenstock and M. Lösche, *Biophys. J.* 60 (1991) 1545.
- [38] M. Lösche, M. Piepenstock, A. Diederich, T. Grünwald, K. Kjaer and D. Vaknin, *Biophys. J.* 65 (1993) 2160.

- [39] C. Naumann, C. Dietrich, A. Behrisch, T.M. Bayerl, M. Schleicher, D. Bucknall and E. Sackmann, *Biophys. J.* 71 (1996) 811.
- [40] M. Fukuto, K. Penanen, R.K. Heilmann, P.S. Pershan and D. Vaknin, *J. Chem. Phys.* 107 (1997) 5531.
- [41] J. Gallant, B. Desbat, D. Vaknin and C. Salesse, *Biophys. J.* 75 (1998) 2888.
- [42] D. Gidalevitz, Z. Huang and S.A. Rice, *Biophys. J.* 76 (1999) 2797.
- [43] D. Gidalevitz, Z. Huang and S.A. Rice, *Proc. Natl. Acad. Sci. U.S.A.* 96 (1999) 2608.
- [44] T.L. Kuhl, J. Majewski, P.B. Howes, K. Kjaer, A. von Nahmen, K.Y.C. Lee, B. Ocko, J.N. Israelachvili and G.S. Smith, *J. Am. Chem. Soc.* 121 (1999) 7682.
- [45] S.J. Johnson, T.M. Bayerl, D.C. McDermott, G.W. Adam, A.R. Rennie, R.K. Thomas and E. Sackmann, *Biophys. J.* 59 (1991) 289.
- [46] A. Schmidt, J. Spinke, T. Bayerl, E. Sackmann and W. Knoll, *Biophys. J.* 63 (1992) 1185.
- [47] S. Krueger, J.F. Ankner, S.K. Satija, C.F. Majkrzak, D. Gurley and M. Colombini, *Langmuir* 11 (1995) 3218.
- [48] G. Fragneto, R.K. Thomas, A.R. Rennie and J. Penfold, *Science* 267 (1995) 657.
- [49] A. Diederich and M. Lösche, In *Protein array: An alternate biomolecular system*, K. Nagayama (Eds.), Japan Scientific Societies Press/Elsevier, Tokyo/Limerick 1997, 205.
- [50] A. Malik, W. Lin, M.K. Durbin, T.J. Marks and P. Dutta, *J. Chem. Phys.* 107 (1997) 645.
- [51] T.L. Kuhl, J. Majewski, J.Y. Wong, S. Steinberg, D.E. Leckband, J.N. Israelachvili and G.S. Smith, *Biophys. J.* 75 (1998) 2352.
- [52] A. Braslau, P.S. Pershan, G. Swislow, B.M. Ocko and J. Als-Nielsen, *Phys. Rev. A* 38 (1988) 2457.
- [53] P.S. Pershan, *Faraday Discuss. Chem. Soc.* 89 (1990) 231.
- [54] M. Lösche, *Habilitationsschrift* [in German], Mainz University, 1994.
- [55] R. Reiter, H. Motschmann, H. Orendi, A. Nemetz and W. Knoll, *Langmuir* 8 (1992) 1784.
- [56] W.H. Press, B.P. Flannery, S.A. Teukolsky and W.T. Vetterling, *Numerical Recipes*, Cambridge University Press, Cambridge 1986
- [57] M.C. Wiener, G.I. King and S.H. White, *Biophys. J.* 60 (1991) 568.
- [58] C.-H. Chou, M.J. Regan, P.S. Pershan and X.-L. Zhou, *Phys. Rev. E* 55 (1997) 7212.
- [59] M.C. Wiener and S.H. White, *Biophys. J.* 59 (1991) 162.

- [60] M.C. Wiener and S.H. White, *Biophys. J.* 61 (1992) 428.
- [61] M.C. Wiener and S.H. White, *Biophys. J.* 61 (1992) 434.
- [62] M. Lösche and H. Möhwald, *J. Colloid Interf. Sci.* 131 (1989) 56.
- [63] C.A. Helm, L.A. Laxhuber, M. Lösche and H. Möhwald, *J. Colloid Polym. Sci.* 264 (1986) 46.
- [64] M. Schalke, Ph.D. thesis, Leipzig University (2000) [in German].